

# Neural Simpletrons – Minimalistic Directed Generative Networks for Learning with Few Labels

Dennis Forster<sup>1\*</sup>, Abdul-Saboor Sheikh<sup>2,3\*</sup>, Jörg Lücke<sup>3</sup>

forster@fias.uni-frankfurt.de, sheikh.abdulsaboor@gmail.com, joerg.luecke@uni-oldenburg.de

<sup>1</sup> Frankfurt Institute for Advanced Studies (FIAS), Frankfurt am Main, Germany

<sup>2</sup> Technical University of Berlin, Berlin, Germany

<sup>3</sup> Carl von Ossietzky University of Oldenburg, Oldenburg, Germany

\*joined first authorship

## Abstract

Deep learning is intensively studied using the perspectives of unsupervised and supervised learning. Comparisons of deep directed generative models and deep discriminative networks is difficult, however, because of: (A) the different semantics of their graphical descriptions; (B) different parameter optimization methods; (C) different benchmarking objectives, and (D) different scalability. Here, we investigate a deep directed model in a form and setting as similar to standard deep neural networks as possible. Based on normalized Poisson mixtures, we derive a minimalistic deep neural network with local activation and learning rules. The network can learn in a semi-supervised setting and can be scaled using standard deep learning tools. Benchmarks with partly labeled data provide the canonical domain for comparison with deep discriminative networks. Empirical evaluations show, that: (A) Performance of the network is competitive with recent deep networks (and other systems). (B) The network can be applied down to the limit of very few labeled data points. (C) The network is the best performing monolithic (i.e., non-hybrid) system for few labels. Our results provide a baseline for more expressive deep directed models, they highlight the performance vs. complexity tradeoff for deep learning, and show that already minimalistic deep directed models are competitive if they can be scaled.

## 1 Introduction

Deep neural networks (DNNs) represent the state-of-the-art in many application domains but they require large and fully labeled data sets. Furthermore, often many free parameters have to be tuned (for architecture, regularization, sparsity etc.). Another class of models, deep directed generative models, represents an alternative with many desirable properties: they offer a principled approach to leverage unlabeled data, they make their used assumptions explicit, are fully interpretable, offer standard meta-algorithms for learning, and they often result in systems with fewer free parameters (e.g., using trainable priors instead of regularization, [Berkes et al. \[2008\]](#), [Mohamed et al. \[2012\]](#), [Sheikh et al. \[2014\]](#), or hyper-priors for architectures, [Adams et al. \[2009\]](#)).

The field of deep learning is, however, not dominated by deep directed models (DDMs) but by DNNs that can classify data with fine-tuned discrimination boundaries. While many different forms of DNNs exist [e.g. [Hinton et al., 2006](#), [LeCun and Bengio, 1995](#), [LeCun et al., 2010](#), [Salakhutdinov and Hinton, 2009](#), [Schmidhuber, 2015](#)], they have in common that back-propagation is decisive for their performance. This is also the case for systems that use unsupervised learning for initial training [[Hinton et al., 2006](#), [Salakhutdinov and Hinton, 2009](#)]. Much of the success of DNNs is owed to drastic performance increases of state-of-the-art computer hardware in combination with large data sets that have been hand-labeled. Current hardware and the scalability of discriminative deep networks can therefore be regarded as their key advantage. It is now common to train deep networks with tens of thousands of neurons [[Schmidhuber, 2015](#)].

While being potentially more powerful information processors, DDMs are typically only trained on smaller scales (either because of computational limits or performance saturation). Deep sigmoid belief networks [SBNs [Saul et al., 1996](#), [Gan et al., 2015](#)] or newer models such as NADE [[Larochelle and Murray, 2011](#)] have only been trained with a couple of hundred to about a thousand hidden units [[Bornschein and Bengio, 2015](#), [Gan et al., 2015](#)]. Even if comparable network sizes for DDMs and DNNs are used, comparison is difficult because (A) DDM units realize different and typically more complex computations per node, and (B) they often use binary or binarized data sets that are evaluated in a fully unsupervised setting [[Larochelle and Murray, 2011](#), [Bornschein and Bengio, 2015](#), [Gan et al., 2015](#)]. Important questions are therefore difficult to answer: How well can large DDMs perform in comparison to DNNs, for instance? Or, how critical for performance is fully probabilistic inference compared to feed-forward classification?

To address such questions, we here investigate a DDM in a form and setting as similar to standard DNNs as possible. We aim at defining the most minimalistic deep directed system, formulated itself in a form of a neural network with compact and local interaction and learning rules but without using back-propagation. The gained similarity to standard neural networks at the same time allows for the application of software tools for parallelization on state-of-the-art GPUs [e.g., [Bastien et al., 2012](#)]. We can in this way scale the system to network sizes comparable to DNNs. The canonical evaluation setting for comparison with standard DNNs (and other approaches) is then given by benchmarks for partly labeled data (semi-supervised learning).

## 2 A hierarchical mixture model for classification

A classification problem can be modeled as an inference task in a probabilistic mixture model. Such a model can be hierarchical or *deep* if we expect the data to obey a hierarchical structure. For hand-written digits, for instance, we first assume the data to be separated by digit classes ('0' to '9') and within each class, we expect structure that distinguishes between different writing styles.

**The Generative Model** Following the hierarchical formulation of a classification problem, we define a minimalistic generative model with layer weights  $(\mathcal{W}, \mathcal{R})$ :

$$p(k) = \frac{1}{K}, \quad p(l|k) = \delta_{lk} \quad (1)$$

$$p(c|k, \mathcal{R}) = \mathcal{R}_{kc}, \quad \sum_c \mathcal{R}_{kc} = 1 \quad (2)$$

$$p(\vec{y} | c, \mathcal{W}) = \prod_d \text{Poisson}(y_d; \mathcal{W}_{cd}), \quad \sum_d \mathcal{W}_{cd} = A \quad (3)$$

The top layer of the model represents  $K$  abstract concepts or super classes  $k$  with labels  $l$  (e.g., digits '0' to '9'). A middle layer is introduced to encapsulate any of the occurring  $C$  subclasses  $c$  (e.g., different writing styles of the digits). The bottom layer represents an observed data sample  $\vec{y}$  generated by the model according to a Poisson distribution, i.e., in line with typical Deep Learning models we assume positive observed data (with Poisson being an elementary non-negative distribution). Note that while the normalization of the rows of  $\mathcal{R}$  is required for normalized categorical distributions, the normalization of the rows of  $\mathcal{W}$  represents an additional constraint of our approach. By constraining the weights to sum to a constant  $A$ , the model expects contrast normalized data. If the dimensionality  $D$  of the observed data is sufficiently large, we can simply normalize the data such that  $\sum_d y_d = A$  in order to fulfill the constraint. With unnormalized data points  $\vec{y}$ , we assume the normalized data points  $\vec{y}'$  to be obtained as follows:

$$y_d = (A - D) \frac{\tilde{y}_d}{\sum_{d'} \tilde{y}_{d'}} + 1 \quad (4)$$

**Maximum Likelihood Learning** Given  $N$  data points  $\vec{y}^{(n)} \in \mathbb{R}_+^D$  and  $\sum_d y_d^{(n)} = A$ , we seek parameters  $\Theta = (\mathcal{W}, \mathcal{R})$  of model eqs. (1) to (3) that maximize the data (log-)likelihood

$$\mathcal{L}(\Theta) = \sum_{n=1}^N \log \left( \sum_{c=1}^C \left( \left( \prod_{d=1}^D \frac{\mathcal{W}_{cd}^{y_d^{(n)}} e^{-\mathcal{W}_{cd}}}{\Gamma(y_d^{(n)} + 1)} \right) \sum_{k \in l^{(n)}} \frac{\mathcal{R}_{kc}}{K} \right) \right). \quad (5)$$

Here we assume that some or all of the data may come labeled. Whenever the label  $l^{(n)}$  is known for a data point  $\vec{y}^{(n)}$ , the summation over  $k$  in eq. (5) gets marginalized to  $R_{lc}$ .

To find likelihood maximizing values of  $\Theta$ , we can apply the Expectation Maximization (EM) algorithm. EM iteratively increases the free-energy, which can be shown to be a tight lower bound of the log-likelihood (see appendix C for details).

**M-step Parameter Updates** The M-step parameter update equations of the model can canonically be derived by maximizing the free energy under the given boundary conditions. Using the method of Lagrange multipliers for constrained optimization, we obtain:

$$\mathcal{W}_{cd} = A \frac{\sum_n p(c|\vec{y}^{(n)}, l^{(n)}, \Theta^{\text{old}}) y_d^{(n)}}{\sum_{d'} \sum_n p(c|\vec{y}^{(n)}, l^{(n)}, \Theta^{\text{old}}) y_{d'}^{(n)}} \quad (6)$$

$$\mathcal{R}_{kc} = \frac{\sum_n p(k|l^{(n)})p(c|\vec{y}^{(n)}, l^{(n)}, \Theta^{\text{old}})}{\sum_{c'} \sum_n p(k|l^{(n)})p(c'|\vec{y}^{(n)}, l^{(n)}, \Theta^{\text{old}})} \quad (7)$$

where only labeled data is taken into account for  $\mathcal{R}_{kc}$  updates.

**E-step Posteriors** For the deep mixture model, the required posteriors over the unobserved latents in eqs. (6) and (7) can be efficiently computed in closed-forms in the E-step:

$$p(c|\vec{y}^{(n)}, l^{(n)}, \Theta^{\text{old}}) = \frac{\exp(I_c^{(n)})}{\sum_{c'} \exp(I_{c'}^{(n)})}, \text{ with} \quad (8)$$

$$I_c^{(n)} = \sum_d \log(\mathcal{W}_{cd}^{\text{old}}) y_d^{(n)} + \log\left(\sum_k u_k^{(n)} \mathcal{R}_{kc}^{\text{old}}\right) \quad (9)$$

$$u_k^{(n)} = \begin{cases} p(k|l^{(n)}) = \delta_{kl^{(n)}} & \text{for labeled data} \\ p(k) = \frac{1}{K} & \text{for unlabeled data} \end{cases} \quad (10)$$

Here, the posteriors  $p(c|\vec{y}, l, \Theta)$  for labeled data and  $p(c|\vec{y}, \Theta)$  for unlabeled data only differ in the chosen distribution for  $u_k$ .

**Probabilistically Optimal Classification** Once we have obtained a set of values for model parameters  $\Theta$  by applying the EM algorithm on training data, we can use the optimized generative model to infer the posterior distribution  $p(k|\vec{y}, \Theta)$  given a previously unseen observation  $\vec{y}$ . For our model this posterior is given by:

$$p(k|\vec{y}, \Theta) = \sum_c \frac{\mathcal{R}_{kc}}{\sum_{k'} \mathcal{R}_{k'c}} p(c|\vec{y}, \Theta), \quad (11)$$

and we can pick the maximum a-posteriori (MAP) value of the distribution for classification.

### 3 A neural network for optimal hierarchical learning

Without diverging from the aforementioned maximum likelihood solution, if we want to transform learning such that it can happen in real-time, e.g., for large-scale or online scenarios, we have to find a valid online regime to replace the batch mode updates eqs. (6) and (7). Another motivation for an online method is its coherence with learning in biological neural circuits; for the hierarchical model in sec. 2, an online learning algorithm can indeed be derived, which can be shown to take a neurally plausible form. To this end, we make use of earlier results in [Lücke and Sahani \[2008\]](#) and [Keck et al. \[2012\]](#), who derived neural online learning

equations that converge to batch-mode EM-based learning in a shallow mixture model [also compare [Nessler et al., 2013](#)]. In this study we extend those results to address the problem of inference and learning in the fully hierarchical generative model given in sec. 2.

**A Neural Network Approximation** Consider the neural network in fig. 1 with neural activities  $\vec{y}$ ,  $\vec{s}$  and  $\vec{t}$ . We assume  $\vec{y}$  to be obtained from a set of unnormalized data points  $\vec{y}$  by [eq. \(4\)](#), and the label information to be presented as top-down input vector  $\vec{u}$  as given in [eq. \(10\)](#). Furthermore, we assume the neural activities  $\vec{s}$  and  $\vec{t}$  to be normalized to  $B$  and  $B'$  respectively (i.e.,  $\sum_d y_d = A$ ,  $\sum_k u_k = 1$ ,  $\sum_d s_c = B$ , and  $\sum_k t_k = B'$ ). For the neural weights  $(W, R)$  of the network (which we distinguish from the generative weights  $(\mathcal{W}, \mathcal{R})$  of the mixture model) we consider Hebbian learning with a subtractive synaptic scaling term :

$$\Delta W_{cd} = \epsilon_w (s_c y_d - s_c W_{cd}) \quad (12)$$

$$\Delta R_{kc} = \epsilon_R (t_k s_c - t_k R_{kc}). \quad (13)$$

By taking sums over  $c$  and over  $k$  respectively, we find that  $\sum_d W_{cd}$  converges to  $A$  and  $\sum_c R_{kc}$  converges to  $B$ . If we now, because of this result, assume the weights  $W$  and  $R$  to be normalized to  $A$  and  $B$  respectively, we can show that an iterative application of online learning in eqs. (12) and (13) finally results in the weights  $W$  and  $R$  to satisfy the following equations at convergence:

$$W_{cd} \approx A \frac{\sum_n s_c^{(n)} y_d^{(n)}}{\sum_d \sum_n s_c^{(n)} y_d^{(n)}}, \quad R_{kc} \approx B \frac{\sum_n t_k^{(n)} s_c^{(n)}}{\sum_c \sum_n t_k^{(n)} s_c^{(n)}}, \quad (14)$$

where  $\vec{y}^{(n)}$  is the  $n$ th data point, and  $\vec{s}^{(n)}$  and  $\vec{t}^{(n)}$  are the hidden neural activities given  $\vec{y}^{(n)}$  and  $\vec{u}^{(n)}$ . [Eqs. \(14\)](#) become exact in the limit of small learning rates  $\epsilon_{w/R}$  in eqs. (12) and (13) and large numbers of data points  $N$ . The derivations are done through a series of approximations including Taylor expansion and the geometric series. Details are given in appendix D.

For the normalization assumptions demanded above, [eqs. \(14\)](#) apply for any neural activation rules for  $s_c$  and  $t_k$  as long as learning converges. For our purposes, we identify  $s_c$  with the posterior probability  $p(c|\vec{y}, l, \Theta)$  for labeled data and  $p(c|\vec{y}, \Theta)$  for unlabeled data, and  $t_k$  with the posterior probability  $p(k|l)$ , all given by the E-step posteriors in eqs. (8) to (10) with  $\theta = (W, R)$ . A comparison of [eqs. \(14\)](#) with M-step eqs. (6) and (7) shows that such neural online learning is equal to EM-learning at convergence (note that  $B = B' = 1$  as  $s_c$  and  $t_k$  sum to one).

Considering eqs. (8) to (10), we can interpret  $I_c$  as input to neural unit  $s_c$ . The input consists of a bottom-up and a

Table 1: Neural network formulation of probabilistic inference and maximum likelihood learning.

Neural Simpletron		
<b>Input</b>		
Bottom-Up:	$\tilde{y}_d$	unnormalized data
		(T1.1)
Top-Down:	$u_k = \begin{cases} \delta_{kl} & \text{for labeled data} \\ \frac{1}{K} & \text{for unlabeled data} \end{cases}$	(T1.2)
<b>Activation Across Layers</b>		
Obs. Layer:	$y_d = (A - D) \frac{\tilde{y}_d}{\sum_{d'} \tilde{y}_{d'}} + 1$	(T1.3)
1 <sup>st</sup> Hidden:	$s_c = \frac{\exp(I_c)}{\sum_{c'} \exp(I_{c'})}$ , with	(T1.4)
	$I_c = \sum_d \log(W_{cd}) y_d + \log(\sum_k u_k R_{kc})$	(T1.5)
2 <sup>nd</sup> Hidden:	$t_k = \begin{cases} \delta_{kl} & \text{for labeled data} \\ \sum_c \frac{R_{kc}}{\sum_{k'} R_{k'c}} s_c & \text{class inference} \end{cases}$	(T1.6)
<b>Learning of Neural Weights</b>		
1 <sup>st</sup> Hidden:	$\Delta W_{cd} = \epsilon_W (s_c y_d - s_c W_{cd})$	(T1.7)
2 <sup>nd</sup> Hidden:	$\Delta R_{kc} = \epsilon_R (t_k s_c - t_k R_{kc})$	(T1.8)

top-down activation. The bottom-up input is the standard weighted summation of neural networks (note that we could redefine the weights by  $\tilde{W}_{cd} := \log(W_{cd})$ ). Likewise, the top-down input is a standard weighted sum,  $\sum_k u_k R_{kc}$ , but affects the input logarithmically. Both sums can be computed locally at the neural unit  $c$ . The inputs to the hidden units  $s_c$  are then combined using a softmax function, which is also standard for neural networks. Here however, the weighted sums as well as the softmax are not imposed ad-hoc, but are a direct result from the generative mixture model.

The other posterior  $p(k|l)$  identified with  $t_k$  assumes labeled data (i.e., like in the M-step of the generative model, we will update the neural weights  $R_{kc}$  only for labeled data). For unlabeled data, we can then identify the activities  $t_k$  with the posterior  $p(k|\vec{y}, \theta)$  given by [eq. \(11\)](#) for class inference.

The complete learning rules for the neural network are given in tab. 1.

The computation of posteriors is in general a difficult and computationally intensive part, and their interpretation as neural activation rules is usually difficult. Because of a specific interplay between introduced constraints, categorical distribution and Poisson noise, the posteriors that have to be computed in our case greatly simplify. And due to the direct correspondence of the derived M-step rules (6) and (7) to the convergence points of neural updates (14),

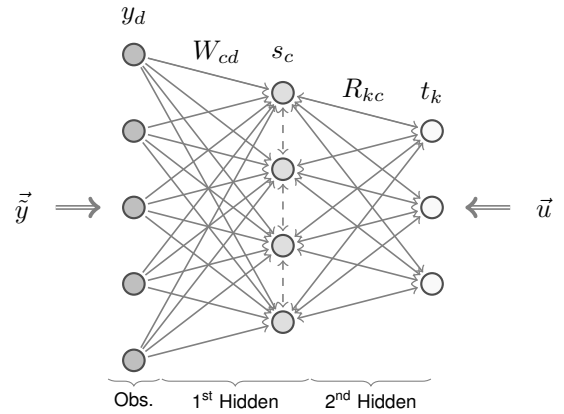


Figure 1: Graphical illustration of the hierarchical recurrent neural network model.

we can directly interpret the neural activations as posterior distributions w.r.t. the hierarchical mixture model of sec. 2. In particular, we can use simple Hebbian learning in (12) and (13) to achieve probabilistic maximum likelihood learning. Though such online learning has the same convergence points as EM learning for the mixture model, in finite distances from the convergence points, neural learning follows different gradients, i.e., the trajectories of the network in parameter space are different from EM. By adjusting the learning rates in eqs. (12) and (13), the gradient directions can be changed in a systematic way without changing the convergence points, which can be used to avoid convergence to early local optima.

Note that the equations defining the neural network are elementary, very compact, and they contain a minimal number of four free parameters:  $\epsilon_w$ ,  $\epsilon_r$  (learning rates), input normalization constant  $A$ , and number of hidden units  $C$ . All numerical experiments will be based on tab. 1, and because of its compactness we call the network *Neural Simpletron* (NeSi).

**Recurrent, Feed-Forward and Greedy Learning** In the experiments, we will refer to our method tab. 1 as r-NeSi ('r' for *recurrent*). To investigate the effect of recurrent information in our network, we also test a feed-forward version, where we disregard the top-down information given by the learned distribution  $p(c|k, R) = R_{kc}$  and always treat this as equal to the prior distribution  $p(c) = 1/C$  in the first hidden layer. Eq. (T1.5) then only contains the first, feed-forward term. This version will be referred to as ff-NeSi ('ff' for *feed-forward*). Since ff-NeSi is stripped of all top-down recurrency, the network can be trained disjointly using a greedy layer-by-layer approach, which is customary for deep networks.

**Semi-Supervised Learning** The second hidden layer of NeSi is trained fully supervised, i.e., it is only updated for data points  $\vec{y}^{(n)}$  for which a label  $l^{(n)}$  is available. However the first hidden layer is trained using all the data, both labeled and unlabeled. While in the feed-forward network the first hidden layer is trained disjointly and fully unsupervised, in the recurrent formulation the network is able to incorporate additional class information flowing-in from the top layer to derive learning into a more discriminative regime.

## 4 Numerical experiments

We apply an efficiently scalable implementation<sup>1</sup> of our network to two widely used benchmarks for classification, the 20 Newsgroups text dataset and the dataset of handwritten digits MNIST. To investigate the task of learning from weakly labeled data, we randomly divide the training parts of the data sets into labeled and unlabeled partitions, where we make sure that each class has the same number of labeled training examples, if possible. We repeat experiments for different proportions of labeled data and measure the classification error on the test set. For the different fractions of labeled data, we report the average classification error computed over 10 independent runs with random labeled and unlabeled data selection.

Details on parallelization, weight initialization and parameter tuning can be found in appendix A. More detailed statistics of the obtained results are given in appendix B.

**Parameter Tuning** Availability of only few labels has to be taken into account as restriction for both training of the model as well as tuning of free parameters. In our experiments we therefore not only train the network in the weakly labeled setting but also tune our free parameters using only the same weakly labeled training data. This way we make sure, that our results are achieved by using no more labels than provided within each training setting and with no additional knowledge about performance on the test set. A detailed explanation of the tuning protocol is given in appendix A.3.

### 4.1 Document Classification (20 Newsgroups)

The 20 Newsgroups dataset in the ‘bydate’ version consists of 18 774 newsgroup documents belonging to 20 different

<sup>1</sup> We use a python 2.7 implementation of tab. 1 which is optimized using Theano to execute on a NVIDIA GeForce GTX TITAN Black GPU. Details can be found in appendix A.1. We have provided the source code and scripts for repeating the experiments discussed here along with the submission.

classes of newsgroup topics, of which 11 269 form the training set and the remaining 7505 form the test set. Each data vector comprises the raw occurring frequencies of 61 188 words in each document. We preprocess the data using tf-idf weighting. No stemming, removals of stop words or frequency cutoffs were applied. We investigate settings of 200, 800 and 2000 labels in total – that is 10, 40 and 100 labels per class, as well as the fully labeled setting.

**Results on 20 Newsgroups** Following the described tuning, training and testing protocol, we find optimal values for the free parameters at  $C = 20$ ,  $A = 80\,000$ ,  $\epsilon_w = 5.0 \times C/N$  and  $\epsilon_r = 0.5 \times K/L$ , where  $N$  denotes the total number of training data points and  $L$  denotes the number of labels. We used this parameter setting with the initialization procedure described in sec. 4 for all results of the NeSi algorithms shown in tab. 2.

We train our model on a 20-class problem without any feature selection. To the best of our knowledge, most methods that report performance on the same benchmark do consider other tasks: They either break the task into binary classification between individual or merged topics, e.g., Cheng et al. [2006], Kim et al. [2014], Wang and Manning [2012], Zhu et al. [2003], and/or perform feature selection, e.g., Srivastava et al. [2013], Settles [2011], for classification. There are, however, works that are compatible with our experimental setup [Larochelle and Bengio, 2008, Ranzato and Szummer, 2008]. A hybrid of generative and discriminative RBMs (HDRBM) are trained by Larochelle and Bengio [2008] using stochastic gradient descent to perform semi-supervised learning. They report results on 20 Newsgroups for both fully and weakly labeled setups. All their model and hyper-parameters are optimized using a validation set of 1691 examples in the fully labeled setting. In the semi-supervised setup 200 examples were used for validation. The classification accuracy of the method is compared in tab. 2.

**Additional Experiments** We also performed experiments with the same parameter setting, but using only one label per class for training. There, the r-NeSi algorithm achieves a test

Table 2: Test error on 20 Newsgroups for different weakly labeled settings using the greedy feed-forward and the recurrent Neural Simpletron

#Labels	ff-NeSi	r-NeSi	HDRBM
200	$30.07 \pm 0.61$	$29.19 \pm 0.44$	
800	$27.64 \pm 0.13$	$27.80 \pm 0.24$	31.8
2000	$27.40 \pm 0.23$	$27.98 \pm 0.20$	
7505	$27.53 \pm 0.21$	$27.99 \pm 0.34$	23.8

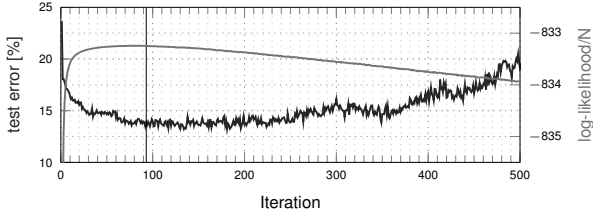


Figure 2: Evolution of test error (black) and log-likelihood (gray) during training. Both show a strong negative correlation. The vertical line denotes the stopping point.

error of  $(67.24 \pm 1.97)\%$  and ff-NeSi of  $(70.91 \pm 2.20)\%$ . For two labels per class, the test error decreases to  $(54.52 \pm 2.10)\%$  for r-NeSi and  $(53.55 \pm 1.92)\%$  for ff-NeSi.

In the fully labeled setting, changing the initialization procedure of r-NeSi to  $R_{kc} = \delta_{kc}$  helped to avoid early local optima and reached a test error of  $(18.40 \pm 0.02)\%$ .

## 4.2 Handwritten Digit Recognition (MNIST)

The MNIST dataset consists of 60 000 training and 10 000 testing data points of  $28 \times 28$  images of gray-scale handwritten digits which are centered by pixel mass. We perform experiments using 100, 600, 1000 and 3000 labels in total as well as the fully labeled training set. Here, we find optima for the free parameters at  $C = 10\,000$ ,  $A = 900$ ,  $\epsilon_w = 0.2 \times C/N$  and  $\epsilon_r = 0.2 \times K/L$ . That is, large networks of 10000 middle layer units are found to perform best.

**A Stopping Criterion Against Overfitting** Training of the first layer in the feed-forward network is not influenced by the state of the second layer, and is therefore oblivious to the number of provided labels. This is no longer the case for the recurrent network. A low number of labels will in the recurrent network lead to overfitting effects when the number of hidden units in the first layer is substantially larger than the number of labeled data points. Since learning in our network corresponds to maximum likelihood learning in a hierarchical generative model, a natural measure to define a criterion for early stopping can be based on monitoring of the log-likelihood (5). As soon as the labeled data starts overfitting the first layer units as a result of top-down influence in  $I_c$ , the log-likelihood computed over the whole training data will start to go down. This declining event in data likelihood can be used as stopping criterion to avoid overfitting. Fig. 2 shows the evolution of the log-likelihood per used data point during training compared to the test error. For experiments over a variety of network sizes, we found strong negative correlations of on average  $\langle \text{PPMCC} \rangle = -0.85 \pm 0.1$ . To

disregard random fluctuations in the likelihood, we compute the centered moving average over 20 iterations and stop as soon as this value drops below its maximum value by more than the centered moving standard deviation. The test error in fig. 2 is only computed for illustration purposes. In our experiments we solely used the moving average of the likelihood to detect the drop event and stop learning. In our control experiments on MNIST we found out that the best test error generally occurred some iterations after the peak in the likelihood (see fig. 2), which we however disregarded in the reported results.

**Results on MNIST** Fig. 4 shows the results of the NeSi algorithms on the MNIST benchmark. As can be observed, the recurrent version (r-NeSi) results in significantly lower classification errors than the feed-forward network (ff-NeSi) in settings with very few labels. In comparison with other standard and recent state-of-the-art approaches our minimalist approaches are competitive – outperforming recent DBN versions and other approaches. In the light of reduced model complexity and effectively used labels, we can furthermore compare to the few algorithms with a lower error rate.

We made a detailed analysis of all algorithms of fig. 4 to analyze complexity, number of free parameters, training, testing and tuning protocols. Comparison details can be found in appendix E. In summary, all algorithms we compare to in fig. 4 are reporting results for a markedly differing (and generally easier) task: they either use the test set for parameter tuning or a validation set with substantially more labels than available during training. Some of the algorithms (namely the TSVM, AGR, AtlasRBF and the Em-networks) also train in a setting, where the (unlabeled) test set is included into the training process. A major problem arises, if such a ‘semi-blind’ approach is compared to a fully blind approach. Deep learning approaches, for instance, usually do not adjust the trainable parameters on the (unlabeled) test data before classification. All semi-blind approaches discussed above do therefore have an advantage, i.e., the comparison is not fair if additional information about the test set is used only by some methods.

Using a validation set can avoid both seeing any test data and having to tune free parameters on the test set. But if this validation set exceeds the training set, then more information is given to an algorithm than what is available during training. In fig. 4 we grouped the models by the number of additional labeled data points used in the validation set for parameter tuning, and fig. 3 shows the performance of the models with respect to the number of labels used solely for training and used for training and parameter tuning combined.

For the NeSi approaches we avoided any training on test

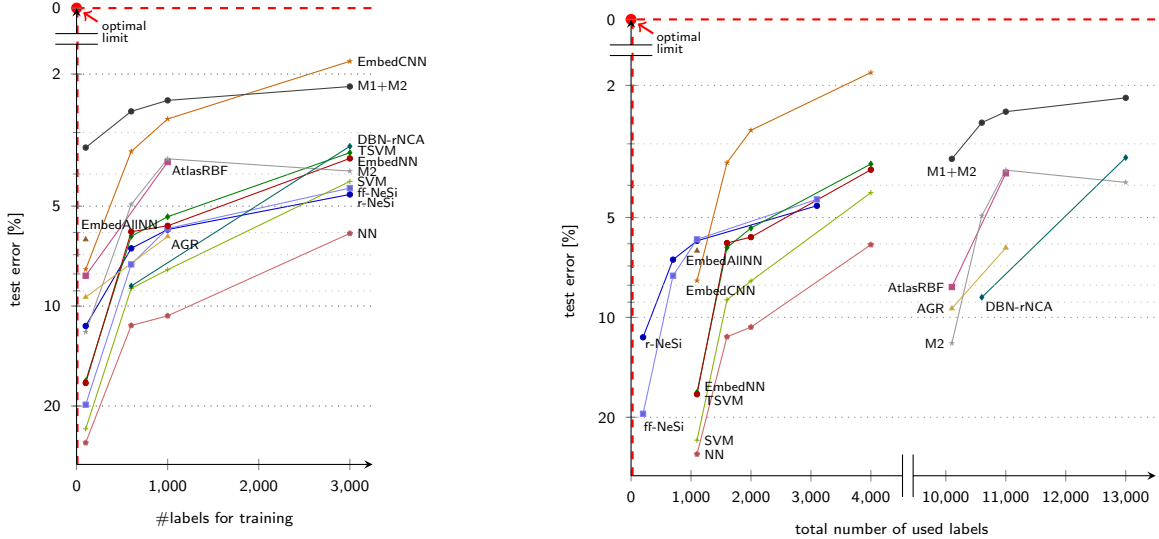


Figure 3: Classification performance of different algorithms compared against varying proportion of weakly labeled training data. The corresponding papers are listed in fig. 4. The left-hand-side plot shows the achieved test errors w.r.t. the amount of labeled data seen by the compared algorithms during training. The right-hand-side plot illustrates for the same experiments the amount of labeled data seen by each of the algorithms when their parameter tuning procedures are also taken into account in conjunction with the training. The plots can be read similar to ROC curves, i.e., the more a curve approaches the upper-left corner, the better is the performance of a system for decreasing amounts of available labeled data.

data and any tuning of free parameters on the test set. Furthermore we made sure, that during parameter tuning no more labels were used than in the training phase.

Since we performed repeated independent training runs to gain meaningful statistical results, and therein used different random label selections with the same parameter setting, we also consider the labels we used during tuning as additional labels, as they are not necessarily a subset of the randomly drawn labels for model training. However, by using as few labels as available during training for parameter tuning, we can assure to be able to find parameter settings for the presented performance using no more labels as given in the respective training settings. Furthermore, this training and tuning schedule assures to not result in an overfitting to the test set. The more free parameters a system uses, the higher the danger of such an overfitting. Therefore, in fig. 4 we also show the number of free parameters for each algorithm, as far as we were able to estimate from the corresponding papers.

In the fully labeled setting, the r-NeSi algorithm achieves a test error of  $(2.95 \pm 0.03)\%$  and the ff-NeSi of  $(3.28 \pm 0.02)\%$ . Training the networks with the same parameter setting with only one label per class, r-NeSi reaches a test error of  $(26.26 \pm 1.59)\%$  and ff-NeSi of  $(54.24 \pm 1.43)\%$ .

## 5 Discussion

While deep directed models (DDMs) represent a model class different from deep neural networks (DNNs), we have shown an example for which inference and learning in a DDM takes a very similar form to learning in standard DNNs. The resulting learning networks, which we termed *simpletrons*, are on the one hand similar to standard DNNs as they learn online, are efficiently scalable, and as their activation rules are local, simple and neurally plausible. On the other hand, simpletrons exhibit features that are a hallmark of deep directed generative models: they can learn from unlabeled data and optimal learning requires integration of bottom-up and top-down information. Eq. (T1.5) for top-down integration and the learning rules eqs. (T1.7) and (T1.8) represent the crucial difference to standard deep learning. The first difference allowed us to study potential benefits of top-down/bottom-up integration in contrast to pure feed-forward. The second difference allows us to study local learning rules approximating likelihood optimization vs. standard back-prop learning. These explicit differences based on a neural network formulation are also the major differences to other generative modeling approaches. Pure generative approaches [such as [Larochelle and Murray, 2011](#), [Bornschein and Bengio, 2015](#), [Gan et al., 2015](#)] are not compared by architecture or performance to DNNs, while, e.g., M1+M2 [[Kingma et al., 2014](#)] is a hybrid ap-

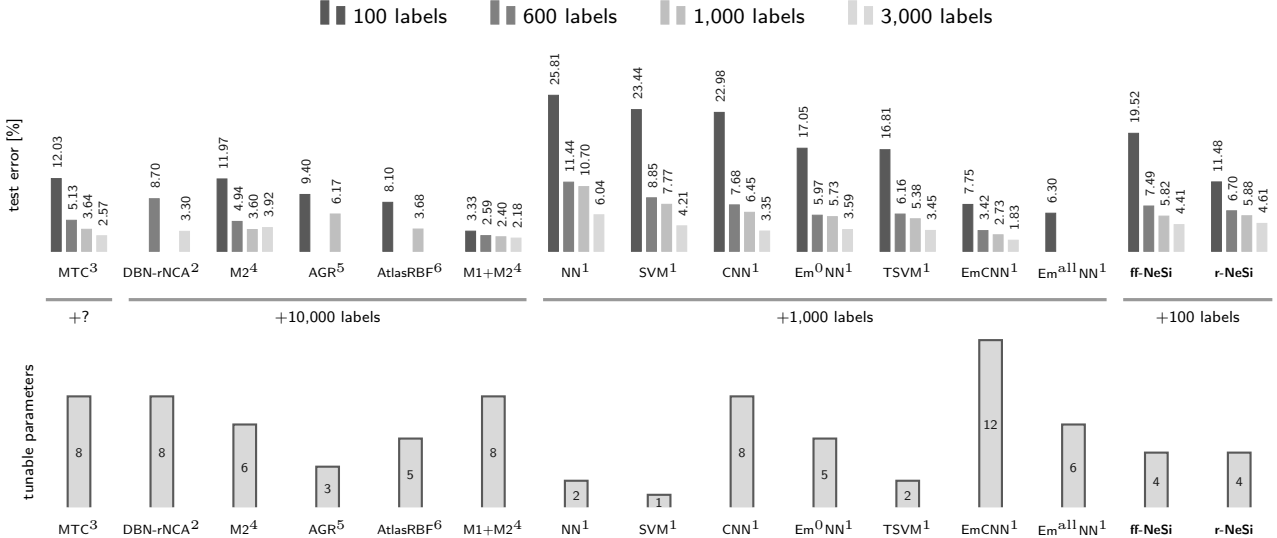


Figure 4: Comparison of different algorithms on weakly labeled MNIST data. The figure shows results for systems, that are trained using 100, 600, 1000, and 3000 labeled MNIST data points. The algorithms are described in detail in the corresponding papers: <sup>1</sup>[Weston et al., 2012], <sup>2</sup>[Salakhutdinov and Hinton, 2007], <sup>3</sup>[Rifai et al., 2011], <sup>4</sup>[Kingma et al., 2014], <sup>5</sup>[Liu et al., 2010], <sup>6</sup>[Pitelis et al., 2014]. The algorithms are of different complexity with different sets of tunable/free parameters (as estimated in tab. E.1). Algorithms also use different training and tuning protocols (appendix E gives more details).

proach which itself contains a DNN using back-prop (making it difficult to highlight differences).

The differences between DDMs and DNNs worked out in this study allow us to answer our initially raised questions using our empirical results:

(1) Deep directed models, if scaled, are competitive to DNNs for weakly labeled data. They outperform all standard DNNs and are competitive with recent specialized state-of-the-art systems.

(2) Probabilistic inference, which results in recurrent bottom-up/top-down integration, has a strong positive impact on performance for weakly labeled data. Performance of a greedy feed-forward system (ff-NeSi) degrades much faster with decreasing label numbers. If the total number of labels required for training *and* parameter tuning is considered, performance of a system with top-down and bottom-up integration (r-NeSi) can maintain a high performance level where performance of other state-of-the-art systems (DNNs, kernel classifiers, and recent hybrid systems) quickly decreases (fig. 3, right-hand-side).

Our comparison of fig. 3 also highlights a performance vs. complexity trade-off which is usually discussed relatively little. If we consider the protocols how the different systems achieve their performance, large differences in the complexity of systems can be noticed. While some systems only need to tune few parameters, others (especially hybrid systems) require tuning of many parameters (fig. 4). Parameter

tuning can be considered as a second optimization loop requiring labels additional to those of the training set. To (partly) normalize for model complexity, performance w.r.t. the total number of required labels could therefore serve as a kind of empirical Occam’s Razor. The NeSi networks, as being derived from a directed model, are amongst the least complex of the competing systems, and the best performing monolithic (non-hybrid) systems for few labels.

In general, the advantage of recurrent integration and the advantage of likelihood optimization vs. discriminative fine-tuning decreases for increasingly many labels. For fully labeled settings, the NeSi systems still perform well but they are not competitive anymore to back-prop based DNNs. Here, fine-tuning of discrimination boundaries is hard to beat. In this respect, the limit of few labels should, however, not be considered as a boundary case. On the contrary, with increasing capabilities of state-of-the-art sensors and data collected through other sources, large data sets are increasingly easy to obtain. Data labels are, on the other hand, costly and often erratic. The very weakly labeled regime is, therefore, arguably the most natural setting for any new application and for high autonomy (also see Collobert et al. [2006], Kingma et al. [2014]).

While our conclusions are based on one example model and standard recent benchmarks for one task, classification, they underline the potential of deep directed generative models, and their far-reaching functional potential in general.

## References

R. P. Adams, H. M. Wallach, and Z. Ghahramani. Learning the structure of deep sparse graphical models. *arXiv preprint arXiv:1001.0160*, 2009.

F. Bastien, P. Lamblin, R. Pascanu, J. Bergstra, I. Goodfellow, A. Bergeron, N. Bouchard, D. Warde-Farley, and Y. Bengio. Theano: new features and speed improvements. *arXiv preprint arXiv:1211.5590*, 2012.

P. Berkes, R. Turner, and M. Sahani. On sparsity and overcompleteness in image models. *Advances in Neural Information Processing Systems*, 21, 2008.

J. Bornschein and Y. Bengio. Reweighted wake-sleep. In *International Conference on Learning Representations (ICLR 2015)*, 2015.

O. Chapelle and A. Zien. Semi-supervised classification by low density separation. In *International Workshop on Artificial Intelligence and Statistics*, 2005.

D. Cheng, R. Kannan, S. Vempala, and G. Wang. A divide-and-merge methodology for clustering. *ACM Transactions on Database Systems (TODS)*, 31(4):1499–1525, 2006.

R. Collobert, F. Sinz, J. Weston, and L. Bottou. Large scale transductive svms. *The Journal of Machine Learning Research*, 7: 1687–1712, 2006.

Z. Gan, R. Henao, D. Carlson, and L. Carin. Learning deep sigmoid belief networks with data augmentation. In *Proceedings AISTATS 2015*, pages 268–276, 2015.

G. Hinton, S. Osindero, and Y. Teh. A fast learning algorithm for deep belief nets. *Neural Computation*, 18:1527–1554, 2006.

C. Keck, C. Savin, and J. Lücke. Feedforward inhibition and synaptic scaling – two sides of the same coin? *PLoS Computational Biology*, 8:e1002432, 2012.

D.-k. Kim, M. Der, and L. K. Saul. A gaussian latent variable model for large margin classification of labeled and unlabeled data. In *AISTATS*, pages 484–492, 2014.

D. P. Kingma, S. Mohamed, D. J. Rezende, and M. Welling. Semi-supervised learning with deep generative models. In *NIPS*, pages 3581–3589, 2014.

H. Larochelle and Y. Bengio. Classification using discriminative restricted boltzmann machines. In *ICML*, pages 536–543, 2008.

H. Larochelle and I. Murray. The neural autoregressive distribution estimator. In *AISTATS*, pages 29–37, 2011.

Y. LeCun and Y. Bengio. Convolutional networks for images, speech, and time-series. In M. A. Arbib, editor, *The Handbook of Brain Theory and Neural Networks*. MIT Press, 1995.

Y. LeCun, K. Kavukcuoglu, and C. Farabet. Convolutional networks and applications in vision. *Proc. Symposium on Circuits and Systems*, pages 253–6, 2010.

W. Liu, J. He, and S.-F. Chang. Large graph construction for scalable semi-supervised learning. In *ICML*, pages 679–686, 2010.

J. Lücke and M. Sahani. Maximal causes for non-linear component extraction. *Journal of Machine Learning Research*, 9:1227–67, 2008.

S. Mohamed, K. Heller, and Z. Ghahramani. Evaluating Bayesian and L1 approaches for sparse unsupervised learning. In *ICML*, 2012.

R. Neal and G. Hinton. A view of the EM algorithm that justifies incremental, sparse, and other variants. In M. I. Jordan, editor, *Learning in Graphical Models*. Kluwer, 1998.

B. Nessler, M. Pfeiffer, L. Buesing, and W. Maass. Bayesian computation emerges in generic cortical microcircuits through spike-timing-dependent plasticity. 2013.

N. Pitelis, C. Russell, and L. Agapito. Learning a manifold as an atlas. In *CVPR*, pages 1642–1649. IEEE, 2013.

N. Pitelis, C. Russell, and L. Agapito. Semi-supervised learning using an unsupervised atlas. In *Machine Learning and Knowledge Discovery in Databases*, pages 565–580. Springer, 2014.

M. Ranzato and M. Szummer. Semi-supervised learning of compact document representations with deep networks. In *ICML*, pages 792–799, 2008.

S. Rifai, Y. N. Dauphin, P. Vincent, Y. Bengio, and X. Muller. The manifold tangent classifier. In *NIPS*, pages 2294–2302, 2011.

R. Salakhutdinov and G. E. Hinton. Learning a nonlinear embedding by preserving class neighbourhood structure. In *AISTATS*, pages 412–419, 2007.

R. Salakhutdinov and G. E. Hinton. Deep boltzmann machines. In *International Conference on Artificial Intelligence and Statistics*, pages 448–455, 2009.

L. K. Saul, T. Jaakkola, and M. I. Jordan. Mean field theory for sigmoid belief networks. *Journal of artificial intelligence research*, 4(1):61–76, 1996.

J. Schmidhuber. Deep learning in neural networks: An overview. *Neural Networks*, 61:85–117, 2015.

B. Settles. Closing the loop: Fast, interactive semi-supervised annotation with queries on features and instances. In *Proceedings of the Conference on Empirical Methods in Natural Language Processing*, pages 1467–1478. Association for Computational Linguistics, 2011.

A.-S. Sheikh, J. A. Shelton, and J. Lücke. A truncated em approach for spike-and-slab sparse coding. *Journal of Machine Learning Research*, 15:2653–2687, 2014.

N. Srivastava, R. R. Salakhutdinov, and G. E. Hinton. Modeling documents with deep boltzmann machines. In *Uncertainty in Artificial Intelligence*, 2013.

S. Wang and C. D. Manning. Baselines and bigrams: Simple, good sentiment and topic classification. In *Annual Meeting of the Association for Computational Linguistics: Short Papers-Volume 2*, pages 90–94, 2012.

J. Weston, F. Ratle, H. Mobahi, and R. Collobert. Deep learning via semi-supervised embedding. In *Neural Networks: Tricks of the Trade*, pages 639–655. Springer, 2012.

X. Zhu, Z. Ghahramani, J. Lafferty, et al. Semi-supervised learning using gaussian fields and harmonic functions. In *ICML*, volume 3, pages 912–919, 2003.

# Appendix

## A More Training Details

### A.1 Parallelization on GPUs and CPUs

The online update rules of the neural network tab. 1 are ideally suited for parallelization using GPUs, as they break down to elementary vector or matrix multiplications. We observed GPU executions with Theano to result in training time speed-ups of over two orders of magnitude compared to single-CPU execution (NVIDIA GeForce GTX TITAN Black GPUs vs. AMD Opteron 6134 CPUs).

Furthermore, we can use the concept of mini-batch training for CPU parallelization or to optimize GPU memory utilization. There, the learning effect of a small number  $\nu$  of consecutive updates is approximated by one parallelized update over  $\nu$  independent updates:

$$\Delta^\nu \omega_{cd}^{(n)} := \epsilon \sum_{i=0}^{\nu-1} \left( f_c(\vec{Y}^{(n+i)}, \omega^{(n)}) Y_d^{(n+i)} - f_c(\vec{Y}^{(n+i)}, \omega^{(n)}) \omega_{cd}^{(n)} \right) \quad (15)$$

$$\omega_{cd}^{(n+\nu)} \approx \omega_{cd}^{(n)} + \Delta^\nu \omega_{cd}^{(n)} \quad (16)$$

The maximal aberration from single-step updates caused by this approximation can be shown to be of  $O((\epsilon\nu)^2)$ . Since this effect is negligible for  $\epsilon\nu \ll 1$ , as experimentally confirmed in tab. A.1, we only consider the mini-batch-size  $\nu$  as a parallelization parameter, and not as free parameter that could be chosen to optimize training in anything else than training speed.

Table A.1: Results are shown as average over 50 training runs on a small network of  $C = 30$  hidden units using  $N = 3000$  training data points of the MNIST dataset. The mini-batch size shows no significant influence neither on the mean nor the variance of the test error or likelihood of the converged solutions.

mini-batch size	1	10	100
mean test error [%]	$23.1 \pm 0.2$	$23.2 \pm 0.2$	$23.0 \pm 0.2$
std. dev. $\sigma_{\text{err}}$ [pp]	1.27	1.26	1.24
mean log-likelihood	$-836.472 \pm 0.005$	$-836.468 \pm 0.005$	$-836.475 \pm 0.005$
std. dev. $\sigma_{\text{ll}}$	0.034	0.032	0.036

### A.2 Weight Initialization

For the complete setting, where there is a good amount of labeled data per hidden unit even in the weakly labeled setting, and the risk of running into early local optima where

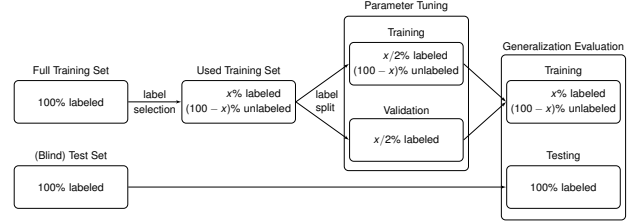


Figure A.1: Parameter tuning, training and testing protocol for the NeSi algorithms.

the classes are not well separated is high, we initialize the weights of the first hidden layer in a modified version of [Keck et al. \[2012\]](#) by computing the mean  $m_{kd}$  and standard deviation  $\sigma_{kd}$  of the labeled training data for each class  $k$  and setting  $W_{kd} = m_{kd} + \mathcal{U}(0, 2\sigma_{kd})$  where  $\mathcal{U}(x_{dn}, x_{up})$  denotes the uniform distribution in the range  $(x_{dn}, x_{up})$ .

For the highly overcomplete setting, where there are far less labeled data points than hidden units in the weakly labeled setting, and class separation is no imminent problem, we initialize the weights using all data disregarding the label information. With the mean  $m_d$  and standard deviation  $\sigma_d$  over all training data points we set  $W_{cd} = m_d + \mathcal{U}(0, 2\sigma_d)$ .

The weights of the second hidden layer are always initialized as  $R_{kc} = 1/C$ .

### A.3 Parameter Tuning Details

To construct the training and validation set for parameter tuning we randomly pick 10 labeled data points per class from the training set (i.e., 100 labeled data points for MNIST and 200 for 20 Newsgroups), which corresponds to the lowest amount of available labeled data points of all here investigated label settings. We take half of this labeled data as validation set and use the other labeled half plus all unlabeled training data as training set in the tuning phase. Once tuned, we keep the free parameters fixed for all following experiments. This ensures a fully blind test set and no additional knowledge in the tuning phase than given in the individual training setting. A more rigorous parameter tuning would also allow for retuning of all parameters for each new label setting, making use of the additional label information in the stronger labeled settings, which we however refrained to do for our purposes. The general tuning, training and testing protocol is shown in fig. A.1.

#### A.3.1 Parameter tuning on 20 Newsgroups

**Hidden units.** For 20 Newsgroups it turned out, that the complete setting, where  $C = K = 20$ , gives the best results

on the validation set. Reasons for this can be the high dimensionality compared to the number of available training data points as well as the prominent noise when taking all words of a given document into account.

**Normalization.** To find a suitable normalization constant  $A$ , we perform experiments for increasing values, starting at  $A \gtrsim D$ , and evaluate the validation error. In the very low regime, the data patterns are for the system indistinguishable from background noise and the validation error is therefore very high. At the other extreme, with very high normalization constants, the softmax function will converge to a winner-take-all maximum function. A good value seems to lie closely after the system is able to distinguish all patterns from background noise but when the normalization is still low enough to allow for a broad softmax response. For all our experiments on the 20 Newsgroups dataset we chose  $A = 80000$ .

**Learning rates.** A relatively high learning rate in the first hidden layer yielded the best results on the validation set. This points to either the system being stopped to early (in every case it stopped by reaching the given maximum number of iterations), or that it converged to a local optimum which is however shallow enough to be overcome by the noise introduced by a bigger ‘step size’ in the movement through parameter space. In any case, we chose  $\epsilon_w = 5.0 \times C/N$  as free parameter setting. We generally express the learning rate as proportional to  $C/N$  for the first hidden layer and proportional to  $K/L$  for the second layer, which represents the learning rate as proportionality factor to the average activation per hidden unit over one full iteration over a dataset of  $N$  data points with  $L$  labels. For the learning rate of the second hidden layer, we chose  $\epsilon_r = 0.5 \times K/L$ .

It is worthy to mention, that the variance using such a small validation set is not negligible and it is well imaginable, that given more experiments the resulting parameter setting could differ from our chosen one, especially in the selection of the learning rates.

### A.3.2 Parameter tuning on MNIST

**Hidden units.** Contrary to the 20 Newsgroup dataset, for MNIST the validation error generally decreases with an increasing number of hidden units. We pick  $C = 10000$  for all our experiments for both the feed-forward and the recurrent network. This represents a good trade-off between performance and required compute time.

**Normalization.** The dependence of the validation error on the normalization constant  $A$  shows similar behavior as for the 20 Newsgroups dataset. Using the same arguments as before, we chose  $A = 900$  for all our experiments on MNIST.

**Learning rates.** While a high learning rate can be used to overcome early local optima, a lower learning rate will in general yield better results with the downside of a longer training time until convergence. This behavior can also be observed on the validation set. As trade-off between performance and training time, we chose  $\epsilon_w = 0.2 \times C/N$  and  $\epsilon_r = 0.2 \times C/N$  for all experiments on MNIST.

## B Detailed Training Results

We performed 10 independent training runs with each network for each label setting with new randomly chosen (class-balanced) labels for each training run. Tabs. B.1 to B.4 give a detailed summary of the statistics of the obtained results. They show the mean test error alongside the error of the mean, the standard deviation (in pp.), as well as the minimal and maximal error in those 10 runs.

Table B.1: r-NeSi on MNIST.

#labels	mean test error	std. dev.	min.	max.
10	$26.26 \pm 1.59$	5.04	21.47	35.10
100	$11.48 \pm 0.33$	1.03	9.70	13.45
600	$6.70 \pm 0.14$	0.45	5.72	7.32
1000	$5.88 \pm 0.07$	0.23	5.57	6.20
3000	$4.61 \pm 0.04$	0.14	4.41	4.78
60000	$2.95 \pm 0.03$	0.08	2.75	3.02

Table B.2: ff-NeSi on MNIST.

#labels	mean test error	std. dev.	min.	max.
10	$54.24 \pm 1.43$	4.53	45.98	59.89
100	$19.52 \pm 0.74$	2.33	16.67	24.14
600	$7.49 \pm 0.16$	0.50	6.92	8.65
1000	$5.82 \pm 0.10$	0.32	5.37	6.55
3000	$4.41 \pm 0.06$	0.18	4.28	4.89
60000	$3.28 \pm 0.02$	0.06	3.21	3.38

Table B.3: r-NeSi on 20 Newsgroups.

#labels	mean test error	std. dev.	min.	max.
20	$67.24 \pm 1.97$	6.23	60.17	75.64
40	$54.52 \pm 2.10$	6.63	38.07	60.97
200	$29.19 \pm 0.44$	1.40	27.28	31.58
800	$27.80 \pm 0.24$	0.76	26.78	29.05
2000	$27.98 \pm 0.20$	0.63	27.24	29.13
7505	$27.99 \pm 0.34$	1.08	26.34	29.82

Table B.4: ff-NeSi on 20 Newsgroups.

#labels	mean test error	std. dev.	min.	max.
20	$70.91 \pm 2.20$	6.95	56.90	79.83
40	$53.55 \pm 1.92$	6.07	38.21	60.76
200	$30.07 \pm 0.61$	1.93	27.99	34.23
800	$27.34 \pm 0.13$	0.40	26.93	28.34
2000	$27.40 \pm 0.23$	0.72	25.98	28.67
7505	$27.53 \pm 0.21$	0.68	26.29	28.69

## C EM for normalized and hierarchical Poisson mixtures

To infer model the parameters  $\Theta = (\mathcal{W}, \mathcal{R})$  of the deep mixture model eqs. (1) to (3) for given a set of  $N$  independent observed data points  $\{\vec{y}^{(n)}\}_{n=1, \dots, N}$  with  $\vec{y}^{(n)} \in \mathbb{R}_+^D$  and  $\sum_d y_d^{(n)} = A$ , and labels  $l^{(n)}$  we seek to maximize the data likelihood  $\mathcal{L} = \prod_{n=1}^N p(\vec{y}^{(n)}, l^{(n)} | \Theta)$  using the Expectation Maximization (EM) algorithm. Instead of maximizing the likelihood directly, EM (in the form studied by [Neal and Hinton \[1998\]](#)) maximizes a lower bound (the free energy) given by:

$$\mathcal{F}(\Theta^{\text{old}}, \Theta) = \sum_{n=1}^N \left\langle \log p(\vec{y}^{(n)}, l^{(n)}, c, k | \Theta) \right\rangle_n + H(\Theta^{\text{old}}) \quad (17)$$

where  $\langle \cdot \rangle_n$  denotes expectation under the posterior

$$\langle f(c, k) \rangle_n = \sum_{c=1}^C \sum_{k=1}^K p(c, k | \vec{y}^{(n)}, \Theta^{\text{old}}) f(c, k) \quad (18)$$

and  $H(\Theta^{\text{old}})$  is an entropy term only depending on parameter values held fixed during the optimization of  $\mathcal{F}$  w.r.t.  $\Theta$ .

The EM algorithm optimizes the free energy by iterating two steps: First, given the current parameters  $\Theta^{\text{old}}$ , the relevant expectation values under the posterior are computed in the E-step; given these posterior expectations,  $\mathcal{F}(\Theta^{\text{old}}, \Theta)$  is maximized w.r.t.  $\Theta$  in the M-step. Iteratively applying E- and M-steps locally maximizes the data likelihood.

## D Approximate equivalence of neural online learning at convergence

In more detail, to derive [eqs. \(14\)](#), we first consider the dynamic behavior of the summed weights  $\bar{W}_c = \sum_d W_{cd}$  and  $\bar{R}_k = \sum_c R_{kc}$ . By taking sums over  $d$  and  $c$  for eqs. (12) and (13) respectively, we obtain

$$\Delta \bar{W}_c = \epsilon_W s_c (A - \bar{W}_c), \quad \Delta \bar{R}_k = \epsilon_R t_k (B - \bar{R}_k). \quad (19)$$

As we assume  $s_c, t_k \geq 0$ , we find that for small learning rates the states  $\bar{W}_c = A$  and  $\bar{R}_k = B$  are stable (and the only) fixed points of the dynamics for  $\bar{W}_c$  and  $\bar{R}_k$ . This applies for all  $k$  and  $c$  and for any  $s_c$  and  $t_k$  that are non-negative and continuous w.r.t. their arguments.

The above result represents a generalization of the result obtained by [Keck et al. \[2012\]](#) applied to two hidden layers instead of one. By assuming normalized weights based on [eqs. \(19\)](#), we can approximate the effect of eqs. (12) and (13) as follows:

$$W_{cd}^{(n+1)} = A \frac{W_{cd}^{(n)} + \epsilon_W s_c(\vec{y}^{(n)}, \Theta^{(n)}) y_d^{(n)}}{\sum_{d'} (W_{cd'}^{(n)} + \epsilon_W s_c(\vec{y}^{(n)}, \Theta^{(n)}) y_{d'}^{(n)})}, \quad (20)$$

and

$$R_{kc}^{(n+1)} = B \frac{R_{kc}^{(n)} + \epsilon_R t_k(\vec{s}^{(n)}, R^{(n)}) s_c(\vec{y}^{(n)}, \Theta^{(n)})}{\sum_{c'} (R_{kc'}^{(n)} + \epsilon_R t_k(\vec{s}^{(n)}, R^{(n)}) s_{c'}(\vec{y}^{(n)}, \Theta^{(n)}))} \quad (21)$$

where  $W^{(n)}$  and  $R^{(n)}$  denote the weights at the  $n$ th iteration of learning, where  $\Theta^{(n)} = (W^{(n)}, R^{(n)})$ , and where  $\vec{s}^{(n)} = \vec{s}(\vec{y}^{(n)}, \Theta^{(n)})$  to abbreviate notation.

Both equations can be further simplified. Using the abbreviations  $F_{cd}^{(n)} = s_c(\vec{y}^{(n)}, \Theta^{(n)}) y_d^{(n)}$  and  $G_{kc}^{(n)} = t_k(\vec{s}^{(n)}, R^{(n)}) s_c(\vec{y}^{(n)}, \Theta^{(n)})$ , we first rewrite eqs. (20) and (21):

$$W_{cd}^{(n+1)} = A \frac{W_{cd}^{(n)} + \epsilon_W F_{cd}^{(n)}}{\sum_{d'} (W_{cd'}^{(n)} + \epsilon_W F_{cd'}^{(n)})} \quad (22)$$

$$R_{kc}^{(n+1)} = B \frac{R_{kc}^{(n)} + \epsilon_R G_{kc}^{(n)}}{\sum_{c'} (R_{kc'}^{(n)} + \epsilon_R G_{kc'}^{(n)})}. \quad (23)$$

Let us suppose that learning has converged after about  $T$  iterations. If we now add another  $N$  iterations and repeatedly apply the learning steps, closed-form expressions for the weights  $W_{cd}^{(T+N)}$  and  $R_{kc}^{(T+N)}$  are given by [eq. \(24\)](#) and [eq. \(25\)](#).

The large products in numerator and denominator of eqs. (24) and (25) can be regarded as polynomials of order  $N$  for  $\epsilon_W$  and  $\epsilon_R$ , respectively. Even for small  $\epsilon_W$  and  $\epsilon_R$  it is difficult, however, to argue that higher-order terms of  $\epsilon_W$  and  $\epsilon_R$  can be neglected because of the combinatorial growth of prefactors given by the large products.

We therefore consider the approximations derived for the non-hierarchical model in [Keck et al. \[2012\]](#), which were applied to an equation of the same structure as eqs. (24) and (25). At closer inspection of the terms  $F_{cd}^{(T+N-n)}$  and  $G_{kc}^{(T+N-n)}$ , we find that we can apply these approximations also for the hierarchical case. For completeness, we reiterate the main intermediate steps of these approximations below:

$$W_{cd}^{(T+N)} = \frac{W_{cd}^{(T)} + \epsilon_W \sum_{n=1}^N F_{cd}^{(T+N-n)} \prod_{n'=n+1}^N (1 + \frac{\epsilon_W}{A} \sum_{d'} F_{cd'}^{(T+N-n')})}{\prod_{n'=1}^N (1 + \frac{\epsilon_W}{A} \sum_{d'} F_{cd'}^{(T+N-n')})} \quad (24)$$

$$R_{kc}^{(T+N)} = \frac{R_{kc}^{(T)} + \epsilon_R \sum_{n=1}^N G_{kc}^{(T+N-n)} \prod_{n'=n+1}^N (1 + \frac{\epsilon_R}{B} \sum_{c'} G_{kc'}^{(T+N-n')})}{\prod_{n'=1}^N (1 + \frac{\epsilon_R}{B} \sum_{c'} G_{kc'}^{(T+N-n')})} \quad (25)$$

$$\prod_{n'=n+1}^N (1 + \frac{\epsilon_W}{A} \sum_{d'} F_{cd'}^{(T+N-n')}) \approx \exp\left(\frac{\epsilon_W}{A} (N-n) \sum_{d'} \hat{F}_{cd'}^{(n)}\right) \quad (26)$$

$$W_{cd}^{(T+N)} \approx \frac{W_{cd}^{(T)} + \epsilon_W \sum_{n=1}^N \exp\left(\frac{\epsilon_W}{A} (N-n) \sum_{d'} \hat{F}_{cd'}^{(n)}\right) F_{cd}^{(T+N-n)}}{\exp\left(\frac{\epsilon_W}{A} N \sum_{d'} \hat{F}_{cd'}^{(0)}\right)} \quad (27)$$

$$\approx \exp\left(-\frac{\epsilon_W}{A} N \sum_{d'} \hat{F}_{cd'}^{(0)}\right) W_{cd}^{(T)} + \epsilon_W \hat{F}_{cd}^{(0)} \sum_{n=1}^N \exp\left(-\frac{\epsilon_W}{A} n \sum_{d'} \hat{F}_{cd'}^{(0)}\right) \quad (28)$$

$$\approx \hat{F}_{cd}^{(0)} \frac{\epsilon_W \exp\left(-\frac{\epsilon_W}{A} \sum_{d'} \hat{F}_{cd'}^{(0)}\right)}{1 - \exp\left(-\frac{\epsilon_W}{A} \sum_{d'} \hat{F}_{cd'}^{(0)}\right)} = A \frac{\hat{F}_{cd}^{(0)}}{\sum_{d'} \hat{F}_{cd'}^{(0)}} = A \frac{\sum_{n=1}^N F_{cd}^{(T+N-n)}}{\sum_{d'} \sum_{n=1}^N F_{cd'}^{(T+N-n)}} \quad (29)$$

Taking [eq. \(24\)](#) as example, we simplify its right-hand-side. The approximations are all assuming a small but finite learning rate  $\epsilon_W$  and a large number of inputs  $N$ . [Eq. \(24\)](#) is then approximated by [eqs. \(27\)](#) to [\(29\)](#), where  $\hat{F}_{cd}^{(n)} = \frac{1}{N-n} \sum_{n'=n+1}^N F_{cd}^{(T+N-n')}$  (note that  $\hat{F}_{cd}^{(0)}$  is the mean of  $F_{cd}^{(n)}$  over  $N$  iterations starting at iteration  $T$ ).

For the first step [\(27\)](#) we rewrote the products in [eq. \(24\)](#) and used the Taylor expansion [\(26\)](#) (see [Supplement of Keck et al. \[2012\]](#) for details).

For the second step [\(28\)](#) we approximated the sum over  $n$  in [\(27\)](#) by observing that the terms with large  $n$  are negligible, and by approximating sums of  $F_{cd}^{(T+N-n)}$  over  $n$  by the mean  $\hat{F}_{cd}^{(0)}$ . For the last steps, [eq. \(29\)](#), we used the geometric series and approximated for large  $N$  (see [Supplement of Keck et al. \[2012\]](#) for details on these last two approximations). Furthermore, we used the fact that for small  $\epsilon_W$ ,  $\frac{\epsilon_W \exp(-\epsilon_W B)}{1 - \exp(-\epsilon_W B)} \approx B^{-1}$  (which can be seen, e.g., by applying l'Hôpital's rule).

By inserting the definition of  $F_{cd}^{(n)}$  into [\(29\)](#) we finally find:

$$W_{cd}^{(T+N)} \approx A \frac{\sum_{n=1}^N s_c(\vec{y}^{(n)}, \Theta^{(T+n)}) y_d^{(n)}}{\sum_{d'} \sum_{n=1}^N s_c(\vec{y}^{(n)}, \Theta^{(T+n)}) y_{d'}^{(n)}}. \quad (30)$$

Analogously, we find for  $R_{kc}$ :

$$R_{kc}^{(T+N)} \approx B \frac{\sum_{n=1}^N t_k(\vec{s}^{(n)}, R^{(T+n)}) s_c^{(n)}}{\sum_{c'} \sum_{n=1}^N t_k(\vec{s}^{(n)}, R^{(T+n)}) s_{c'}^{(n)}}, \quad (31)$$

where we again used  $\vec{s}^{(n)} = \vec{s}(\vec{y}^{(n)}, \Theta^{(T+n)})$  for better

readability in the last equation. If we now assume convergence, we can replace  $W_{cd}^{(T+N)}$  by  $W_{cd}$  and  $R_{kc}^{(T+N)}$  by  $R_{kc}$ , and we recover [eqs. \(14\)](#) in [sec. 3](#) with converged weights  $W_{cd}$  and  $R_{kc}$ .

Note that each approximation is individually very accurate for small  $\epsilon_W$  and large  $N$ . [Eqs. \(14\)](#) can thus be expected to be satisfied with high accuracy in this case and numerical experiments based on comparisons with EM batch-mode learning verified such high precision.

## E More details on the compared algorithms including their testing protocols

In the comparison of [Sec. 4](#), SVM is a standard support vector machine and TSVM a version scalable to larger data sets and applicable in the semi-supervised setting [[Collobert et al., 2006](#)]. Free parameters come in the form of kernel parameters, balancing constraint, parameters for preprocessing and auxiliary algorithms if applicable. In the case of the TSVM the free parameters are explicitly discussed in the paper. For small-scale experiments, [Collobert et al. \[2006\]](#) explicitly state for the TSVM that all its free parameters are tuned on the test set, and they refer to [Chapelle and Zien \[2005\]](#) to motivate such a protocol for algorithm comparison. For training on unlabeled data, the TSVM uses the *test set* and only in cases of more than 10,000 unlabeled data, the training set is added. This means that TSVM has seen the test set data points before classification.

For parameter tuning TSVM uses a validation set (part of the training set) of 1,000 data points.

AGR (or AnchorGraphReg) is an efficient graph construction algorithm used for data classification [Liu et al., 2010]. For MNIST, AGR seems to require relatively few free parameters for: graph regularization, sparsity, number of anchor points, number of nearest anchors, or dimensionality of PCA dimensionality reduction. Importantly, for the reported results in Sec. 4, AGR uses training *and* test set for training. The authors write “We hold the [MNIST] training and test samples as a whole and randomly choose labeled samples from the whole set.” This implies that the algorithm has seen test data and probably at least some of its labels for training before it is evaluated (presumably on the standard test set).

MTC, AtlasRBF, Em<sup>o</sup>NN, Em<sup>all</sup>NN<sup>1</sup>, and EmCNN are approaches that first aim to learn low-dimensional manifolds by using labeled and unlabeled data points before test data is classified. AtlasRBF [Pitelis et al., 2014] combines, for instance, a manifold learning approach [Pitelis et al., 2013] with a support vector classifier. It represents the algorithm with the best results for MNIST among a number of classifier/manifold learning combinations investigated. The free parameters of AtlasRBF consist for the manifold learning part of: manifold dimensionality, a weight sparsity penalty, and number of nearest neighbors that are taken into account. For the classification part, SVM kernel parameters are tuned. For the training and testing it is stated [Pitelis et al., 2014] that AtlasRBF uses the same protocol as AGR [Liu et al., 2010], i.e., the algorithm presumably sees test data points (and some of their labels) before testing.

MTC also learns low-dimensional manifold structure [Rifai et al., 2011] combined with stochastic gradient descent for supervised learning of a neural network classifier. For the results reported in [Rifai et al., 2011] a validation set is used for free parameter tuning. The size of the validation set is not given.

Em<sup>o</sup>NN, Em<sup>all</sup>NN<sup>1</sup>, and EmCNN as well as all data on MNIST in Weston et al. [2012] use the same training and testing protocol as used for the TSVM in Collobert et al. [2006]. This means that: unlabeled test data has been seen and used by the algorithms before the test performance is measured; and that free parameters were presumably tuned on the validation set of 1,000 data points.

The M2 model of Kingma et al. [2014] combines a generative model approach with a deep neural network to connect hidden to observed variables. Free parameters include learning rate, first order decay and second order decay parameters for weights. We found no statement on the hyper-/free-parameters of the used deep neural network architecture in the paper, and no mentioning of a validation set. The source code published together with the paper [Kingma et al., 2014] does contain a validation set of

10,000 data points, however. We therefore used such a validation set for comparison in Sec. 4.

The model M1 also reported in Kingma et al. [2014] is a latent variable model for feature learning combined with a deep network and a classifier such as TSVM but we found it difficult to deduce details on free parameters and tuning protocols. The models M1 and M2 can themselves be combined representing a large heterogeneous system with many free parameters.

The DBN-rNCA approach combines Neighbourhood Component Analysis (NCA) with deep Restricted Boltzmann Machines [Salakhutdinov and Hinton, 2007]. A typical setup consists of four layers (three hidden) for encoding and four layers (three hidden) for decoding and a middle layer, with an architecture for MNIST being (500, 500, 2000, 30, 2000, 500, 500) for the number of hidden units from bottom to top respectively. For the reported results, a set of 10,000 data points taken from the training set was used as validation set.

The discriminative RBM [Larochelle and Bengio, 2008] that we used for comparison of the 20 Newsgroups data also provides a result on MNIST. For 800 labeled training points and a validation set of 200 labeled data points, the semi-supervised “semi-sup HDRBM” results in a test error of 8.04%. This is in the range of the standard SVM of Sec. 4 but note that just 5,000 unlabeled data points were used for training (we therefore did not include this test error in Sec. 4).

In summary, the protocols to train, tune and test the algorithms compared to in Sec. 4 are unfortunately very diverse. Data is deduced from the papers where the classification errors used for Sec. 4 are reported. Also sometimes protocols had to be inferred from context. In general, the deduced data was done to the best of our knowledge but we found it to be a very difficult task. The list is not exhaustive but we believe that we included the currently best performing algorithms according to the reported test error.

## E.1 Tunable hyper-parameters of the compared algorithms

Here we list in tab. E.1 different hyper-parameters used by each of the methods compared in figs. 3 and 4. For most of the methods, the estimate provided here only gives a lower-bound on the number of tunable parameters, as many of them may have multiple instances e.g., for each added layer in the network.

Table E.1: Tunable hyper-parameters of the algorithms compared on the MNIST dataset.

METHOD	TUNABLE HYPER-PARAMETERS	TOTAL
CNN	Patch size, pooling window size (2 <sup>nd</sup> layer), neighborhood radius (4 <sup>th</sup> layer), 1 <sup>st</sup> , 3 <sup>rd</sup> , 5 <sup>th</sup> and 6 <sup>th</sup> layer units, learning rate	8
MTC	$\lambda$ (Jacobian penalty), $\gamma$ (Hessian penalty), number of samples for stochastic estimate of the Hessian, learning rate, number of layers, number of hidden units (per layer), tangent distance penalty, number of tangents	$\geq 8$
DBN-rNCA	RBM learning rate, momentum, weight-decay, RBM epochs, NCA epochs, $\lambda$ (tradeoff parameter), number of layers, number of hidden units (per layer)	$\geq 8$
M2	$\alpha$ , RMSProp parameters: learning rate, first and second momenta, MLP Parameters: number of layers, number of hidden units	6
AGR	$m, s, \gamma$ , dimensionality reduction (for acceleration)	3 – 4
AtlasRBF	$\lambda, \gamma, \sigma$ , number of neighbors, local manifold dimensionality	5
M1+M2	Number of samples from posterior, M2 parameters, MLP Parameters: number of layers, number of hidden units (per layer)	$\geq 8$
NN	Learning rate, number of hidden units	2
SVM	C (soft margin parameter)	1
Em <sup>0</sup> NN	$\lambda, m$ (distance parameter), NN parameters $\times$ number of NN layers	$\geq 5$
TSVM	C(soft margin parameter), $\lambda$ (data-similarity kernel parameter)	2
EmCNN	$\lambda$ (per embedded layer), Number of layers to embed, $m$ (distance parameter), number of CNN layers, CNN parameters	$\geq 12$
Em <sup>all</sup> NN	$\lambda$ (per embedded layer), Number of layers to embed, $m$ (distance parameter), number of NN layers, NN parameters	$\geq 6$
ff-NeSi	A (normalization constant), C (number of middle layer units), $\epsilon_W$ and $\epsilon_R$ (learning rates of 1 <sup>st</sup> and 2 <sup>nd</sup> hidden layer)	4
r-NeSi	A (normalization constant), C (number of middle layer units), $\epsilon_W$ and $\epsilon_R$ (learning rates of 1 <sup>st</sup> and 2 <sup>nd</sup> hidden layer)	4